iScience

CellPress
OPEN ACCESS

Article

Glutamine supplementation reverses manganese neurotoxicity by eliciting the mitochondrial unfolded protein response

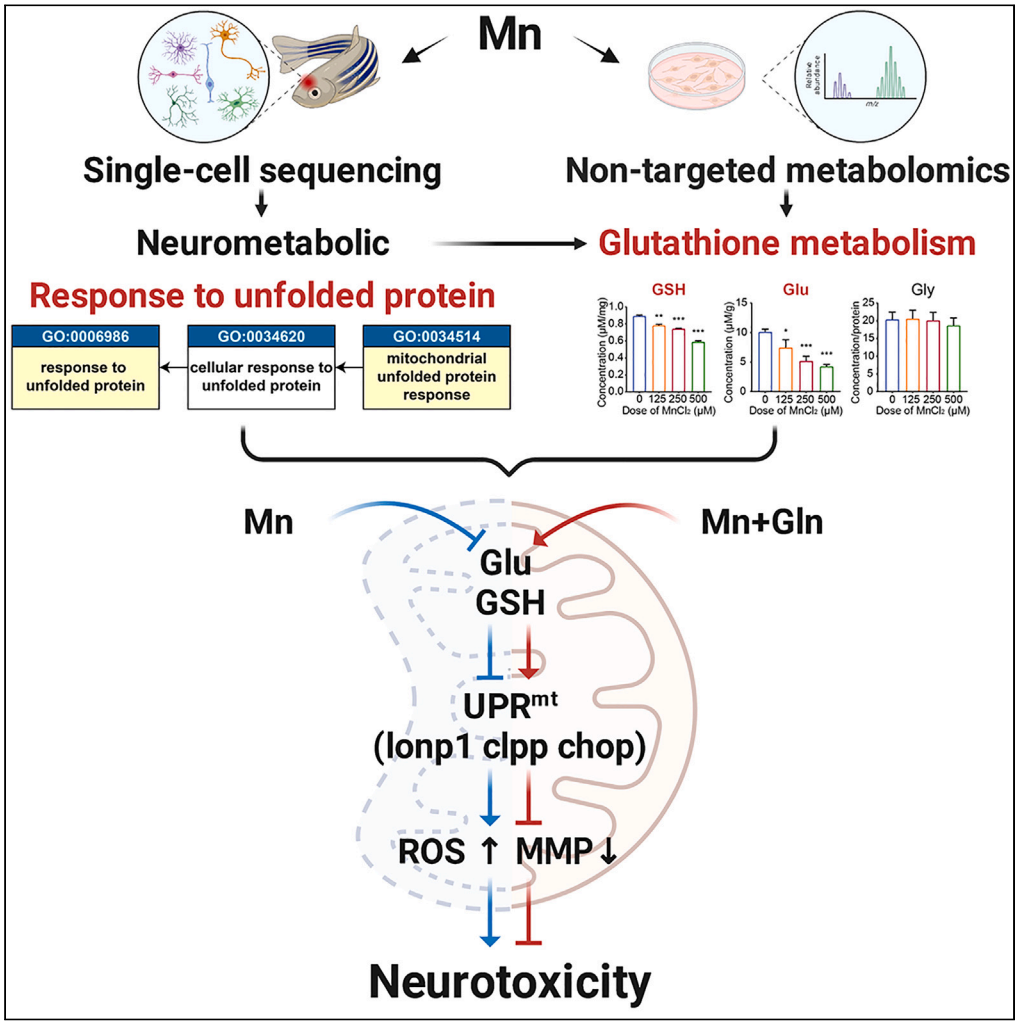

Shixuan Zhang, Junrou Zhang, Luli Wu, Li Chen, Piye Niu, Jie Li

niupiye@ccmu.edu.cn (P.N.)
lijie46@ccmu.edu.cn (J.L.)

Highlights

Mn alters the single-cell transcriptome and amino acid metabolome in the zebrafish brain

Mn inhibits glutathione metabolism and UPR^{mt} leading to mitochondrial dysfunction

Gln supplementation can reverse Mn neurotoxicity by eliciting UPR^{mt}

Zhang et al., iScience *26*, 107136
July 21, 2023
https://doi.org/10.1016/j.isci.2023.107136

iScience

CellPress
OPEN ACCESS

Article

Glutamine supplementation reverses manganese neurotoxicity by eliciting the mitochondrial unfolded protein response

Shixuan Zhang,[1,2,3] Junrou Zhang,[1,2] Luli Wu,[1,2] Li Chen,[1,2] Piye Niu,[1,2,*] and Jie Li[1,2,4,*]

SUMMARY

Excessive exposure to manganese (Mn) can cause neurological abnormalities, but the mechanism of Mn neurotoxicity remains unclear. Previous studies have shown that abnormal mitochondrial metabolism is a crucial mechanism underlying Mn neurotoxicity. Therefore, improving neurometabolic in neuronal mitochondria may be a potential therapy for Mn neurotoxicity. Here, single-cell sequencing revealed that Mn affected mitochondrial neurometabolic pathways and unfolded protein response in zebrafish dopaminergic neurons. Metabolomic analysis indicated that Mn inhibited the glutathione metabolic pathway in human neuroblastoma (SH-SY5Y) cells. Mechanistically, Mn exposure inhibited glutathione (GSH) and mitochondrial unfolded protein response (UPR^{mt}). Furthermore, supplementation with glutamine (Gln) can effectively increase the concentration of GSH and triggered UPR^{mt} which can alleviate mitochondrial dysfunction and counteract the neurotoxicity of Mn. Our findings highlight that UPR^{mt} is involved in Mn-induced neurotoxicity and glutathione metabolic pathway affects UPR^{mt} to reverse Mn neurotoxicity. In addition, Gln supplementation may have potential therapeutic benefits for Mn-related neurological disorders.

INTRODUCTION

Manganese (Mn) is an essential heavy metal and is widely used for multiple industrial purposes. Workers are exposed to Mn in the occupational setting through inhalation of fine dust from welding or smelting.[1] Overexposure to Mn correlates with neurological abnormalities, including effects on behavior, memory deficits, and motor function, which can lead to manganism.[2,3] Mn-induced neurotoxicity has also been associated with a higher risk of developing neurodegenerative diseases including Parkinson's disease (PD) and Alzheimer's disease.[4]

Abnormal metabolism in mitochondria is a critical mechanism of neurotoxicity induced by overexposure to Mn. Mn can cross the blood-brain barrier and accumulate in the putamen, caudate nucleus, and globus pallidus.[5] In the brain, the dopaminergic (DA) neuron was the main target cell of Mn exposure.[6,7] Mitochondria are the powerhouse of brain cells. Mn exposure can lead to mitochondrial dysfunction including inhibition of mitochondrial respiration, reduction of mitochondrial membrane potential (MMP), reactive oxygen species (ROS) accumulation, and mitochondrial oxidative stress.[8] Meanwhile, Mn can perturb intracellular metabolism. Exposure to physiological Mn increases neuroprotective amino acid metabolites such as creatine, phosphocreatine, and phosphoserine in human neuroblastoma (SH-SY5Y) cells, but excess Mn can cause abnormalities in glycerophospholipid metabolism, fatty acid activation, and linoleic acid metabolism.[9,10]

Meanwhile, excess Mn can affect amino acid metabolites. Glutamine (Gln) is known as the most abundant amino acid in the human body. It is of great importance to intermediary metabolism, nitrogen exchange via ammonia, and pH homeostasis.[11] Gln also plays an important role in antioxidant and cytoprotective effects. Gln is synthesized from ammonium and glutamate (Glu). Glu is a component of glutathione (GSH), which is an oxidative scavenger widely present in neuronal mitochondria.[12] A previous study showed that reduced Mn intake significantly increased Gln and Glu levels in the brain tissue of type C hepatic encephalopathy rats.[9] Mn can also disrupt the synthesis of GSH in the brain and result in oxidative damage.[13] However,

[1]Department of Occupational and Environmental Health, School of Public Health, Capital Medical University, Beijing 100069, China

[2]Beijing Key Laboratory of Environmental Toxicology, Capital Medical University, Beijing 100069, China

[3]Department of Nutrition, Beijing Chaoyang Hospital, Capital Medical University, Beijing 100020, China

[4]Lead contact

*Correspondence: niupiye@ccmu.edu.cn (P.N.), lijie46@ccmu.edu.cn (J.L.)

https://doi.org/10.1016/j.isci.2023.107136

evidence of between excess Mn and Gln metabolism is limited, and the underlying mechanism remains unknown.

In the current investigation, we employed adult zebrafish and human neuroblastoma cell line SH-SY5Y as animal and cellular models, respectively. Although *Caenorhabditis elegans* and Drosophila have been used to characterize the molecular mechanisms of Mn-induced neurotoxicity,[14,15] zebrafish is a vertebrate model that possesses both neurological features and the genome contains homologous sequences for approximately 80% of human genes.[16] Zebrafish have emerged as an excellent model for revealing cellular heterogeneity. The single-cell transcriptomic profiles of zebrafish have been extensively used to explore embryonic development, neurogenesis, and adult zebrafish immune system.[17] In addition, zebrafish behavioral and histopathological alterations can be observed to assess neurotoxicity.[18,19] SH-SY5Y cells have been widely utilized as DA neuronal cell models for PD because of their ability to express features of DA neurons, such as dopamine-β-hydroxylase and tyrosine hydroxylase expression, as well as dopamine transporter activity.[20]

Thus, using single-cell sequencing (scRNA-seq), we found that neurometabolic pathways and response to the unfolded protein in mitochondria were altered in DA neurons of zebrafish exposed to Mn. Further metabolomic analysis revealed mitochondrial glutathione metabolism is the key pathway induced by overexposure to Mn. Mechanistically, we used Gln as supplementation to increase the intracellular GSH levels and observed Gln can reverse Mn neurotoxicity by activating UPR^{mt}. Our work highlights the importance of using Gln as a therapeutic strategy for Mn-related neurological disorders.

RESULTS

Mn impaired behavioral and cognitive functions in zebrafish

According to the drinking-water quality guidelines of WHO, the assumed safe dose of Mn in drinking water is 0.4 mg/L. In this study, zebrafish were exposed chronically to 0.25, 1, and 4 mg/L $MnCl_2$ (actual Mn^{2+} concentrations were approximately 0.1, 0.4, and 1.6 mg/L). There was no statistical difference in body weight compared to control in both male and female zebrafish after Mn exposure for 30 d (Figure S1: Body weight of male and female zebrafish exposed to $MnCl_2$ for 30 d (n = 5), related to Figure 1). Figures 1A–1D showed the behavioral and cognitive functions detected by T-maze in zebrafish exposed to Mn. We observed the dose-response relationship between the total swimming distance of both male and female zebrafish with the doses of Mn exposure (Figure 1A). As shown in Figure 1B, zebrafish swimming velocity in the 1 and 4 mg/L $MnCl_2$ groups were significantly reduced than in the control group ($p < 0.05$). The cumulative time in the EC zone was not significantly different in any of the groups except for 4 mg/L $MnCl_2$ in male zebrafish (Figure 1C). The latency time of zebrafish entering the EC zone was significantly prolonged in male and female zebrafish in the 1 and 4 mg/L $MnCl_2$ groups compared to the control in Figure 1D.

Meanwhile, the pathological results showed that the neurons in the brain tissue were morphologically intact, densely structured, and well-arranged in untreated zebrafish, while with increasing doses of Mn exposure, neurons were sparse and disordered in the arrangement (Figure 1E). Neurons in the same part of the zebrafish brain tissue observed under a 50× electron microscope contain 227, 199, 153, and 131 normal neurons in each exposed group in males, and 298, 305, 229, and 177 in females, respectively. Taken together, these observations implied that Mn could cause brain tissue damage in zebrafish, resulting in behavioral and cognitive dysfunction in zebrafish.

Mn exposure affected mitochondrial function, amino acid metabolism pathways, and unfolded protein in zebrafish DA neurons

To find out the main pathway affected by Mn exposure, we evaluated changes in neuronal cell types in zebrafish brain tissue exposed to Mn for 30 d by single-cell sequencing and identified 10 cell types, including cholinergic neurons, DA neurons, glutaminergic neurons, GABAergic neurons, neuronal precursors, and some unidentified neurons, and glial cells including microglia, oligodendrocyte, radial glia, in addition to a group of unidentified cells (Figure 2A). As reported by a previous study[7], Mn exposure caused severe damage to DA neurons and resulted in learning and memory impairment. Therefore, we sorted out DA neurons in zebrafish brain tissue for analysis and found that GO enrichment of DEGs in DA neurons was mainly associated with protein, amino acid, and energy metabolism, cell cycle, and response to unfolded protein (Figure 2B). The KEGG pathway analysis in Figure 2C showed that Mn exposure affected signaling pathways such as oxidative phosphorylation, glutathione metabolism, glycolysis, autophagy, and

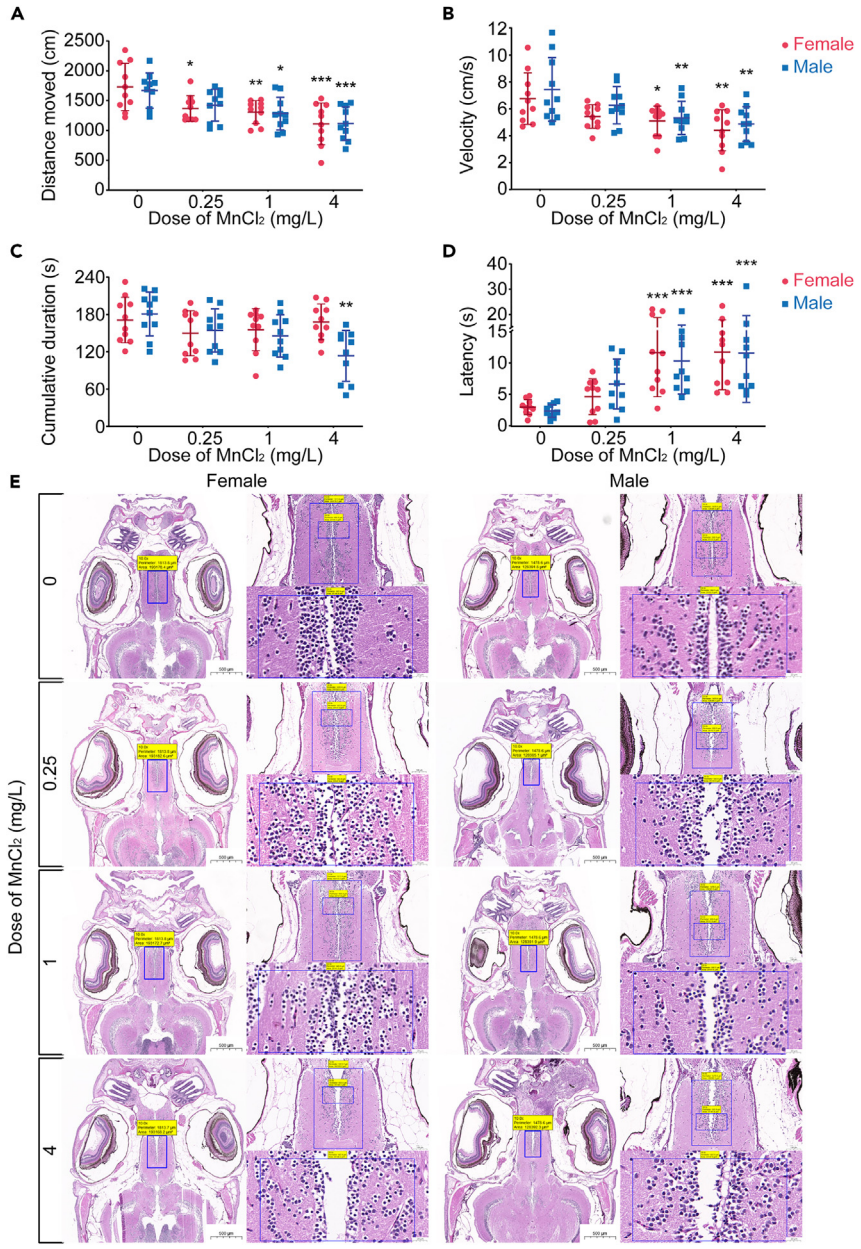

Figure 1. Mn impaired the central nervous system of zebrafish

The total distance (A), average velocity (B), cumulative duration in EC zone (C) and latency time in EC zone (D) of zebrafish in T-maze after 30 days of Mn exposure (n = 10). (E) Pathological changes of brain tissue in zebrafish after Mn exposure for 30 d. Scale bar, 500 μm, 100 μm, and 20 μm. Data were represented as mean ± SD. Experimental significance was determined by one-way ANOVA (*p<0.05; **p<0.01; ***p<0.001).

apoptosis. Collectively, these results suggested Mn exposure affected the metabolism and mitochondrial function of DA neurons in zebrafish, which was further verified at the cellular level.

Mn caused mitochondrial dysfunction and inhibited UPR^{mt} in SH-SY5Y cells

We first determined the cellular activity of SH-SY5Y cells after treatment with 0, 62.5, 125, 250, 500, and 1000 μM $MnCl_2$ for 3, 6, 12, and 24 h (Figure 3A). The treatment conditions (125, 250, and 500 μM of $MnCl_2$ for 6 h) with cell survival above 70% were selected for subsequent experiments. Second, we detected mitochondrial function by flow cytometry, and the results showed that Mn exposure could increase ROS

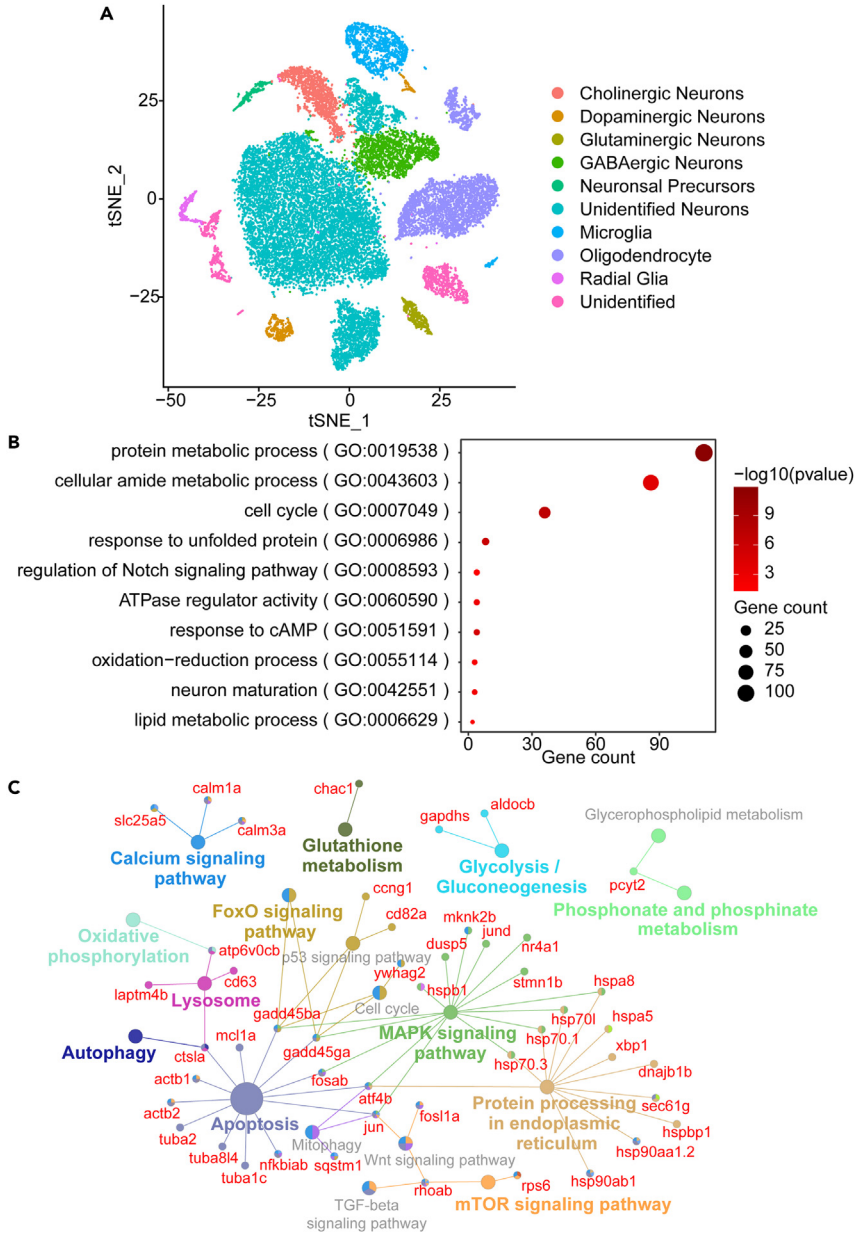

Figure 2. Whole-brain single-cell sequencing and enrichment analysis of DEGs in DA neurons of zebrafish after Mn exposure for 30 d

(A) The tSNE plot of zebrafish brain tissue cell subtypes.

(B) The bubble plot of GO enrichment analysis of DEGs in DA neurons.

(C) The network of KEGG pathway analysis.

levels in Figure 3B. As shown in Figure 3C, the MMP depolarization level showed a dose-dependently increase with Mn exposure. In addition, to verify protein folding participating in Mn neurotoxicity, we determined the protein expression of UPR^{mt}-related protein and the results indicated that the expression of chop was significantly increased in the 125 μM $MnCl_2$ group and showed a decreased trend with increasing Mn exposure concentration in Figure 3D. The expression of clpp protein was decreased significantly in 250 and 500 μM $MnCl_2$ groups, while lonp1 protein expression was significantly decreased compared with the untreated group (all $p<0.05$). The above results indicated that Mn caused mitochondrial dysfunction in

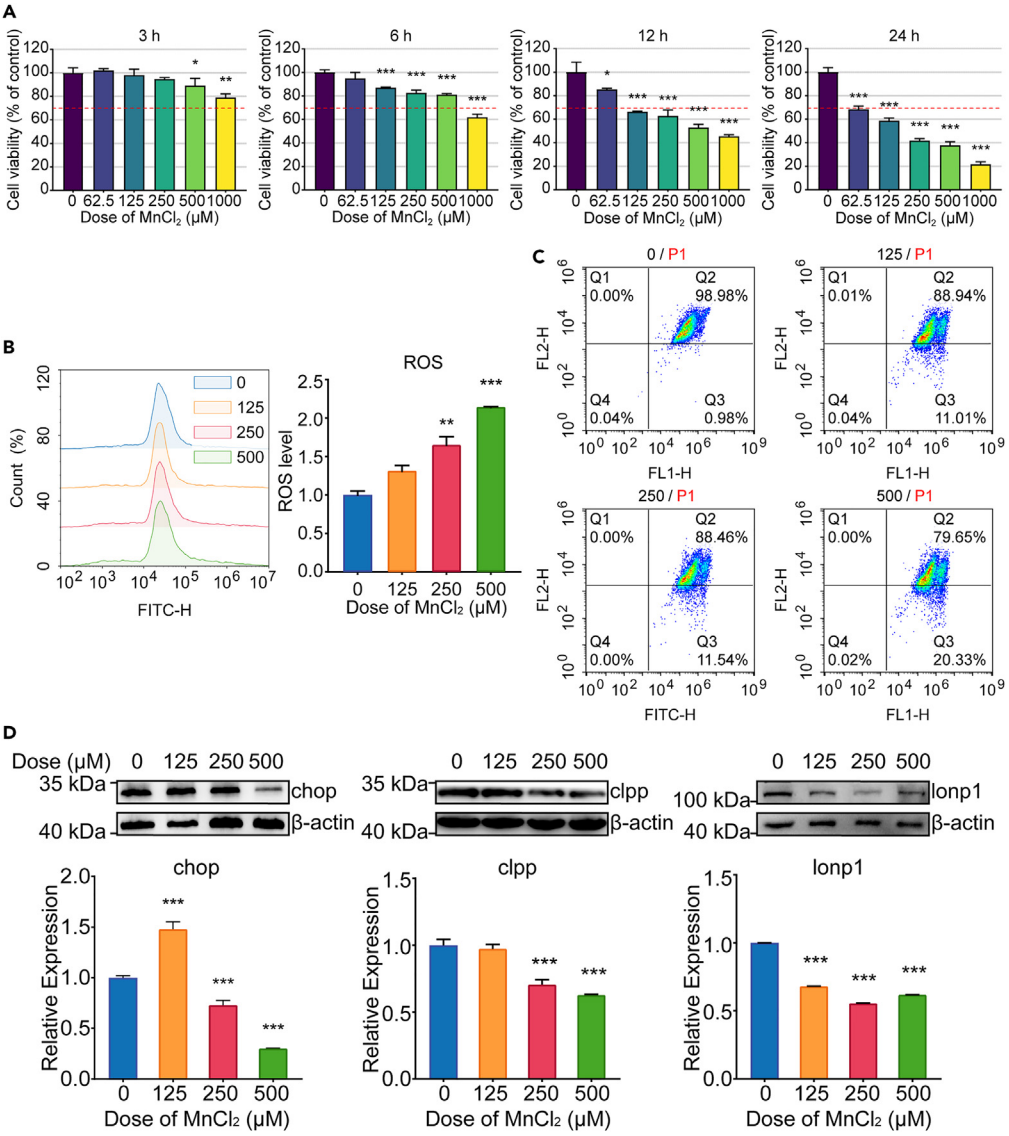

Figure 3. Mn exposure caused neurotoxicity and mitochondrial dysfunction in SH-SY5Y cells

(A) The cell viability of SH-SY5Y cells after Mn exposure was assessed using CCK kit and measured by a microplate reader (n = 6).

The levels of ROS (B) and MMP (C) were measured using flow cytometry (n = 3).

(D) The expression levels of UPR^{mt}-related protein (chop, clpp, and lonp1) after dose-dependent of Mn were used for western blot and were quantified using ImageJ (n = 3). Data were represented as mean ± SD. *$p < 0.05$, **$p < 0.01$, ***$p < 0.001$ versus the control.

SH-SY5Y cells accompanied by increased ROS levels and decreased MMP, moreover, Mn could suppress UPR^{mt}.

Mn neurotoxicity altered mitochondrial glutathione metabolism in SH-SY5Y cells

We further used non-targeted metabolic techniques to establish the metabolome alterations in SH-SY5Y cells after exposure to Mn. The PCA results showed that 34.8% and 33.1% of the characteristics of the original dataset on the PC1 and PC2 dimensional maps could be explained in the positive (ESI$^+$), and negative (ESI$^-$) ion mode, with a clear trend of separation between groups. The pooled QC samples clustered together in the PCA plots in both positive and negative ion modes, indicating stability and repeatability of the analysis system (Figures 4A and 4B). Peaks were aligned, and missing values were eliminated from

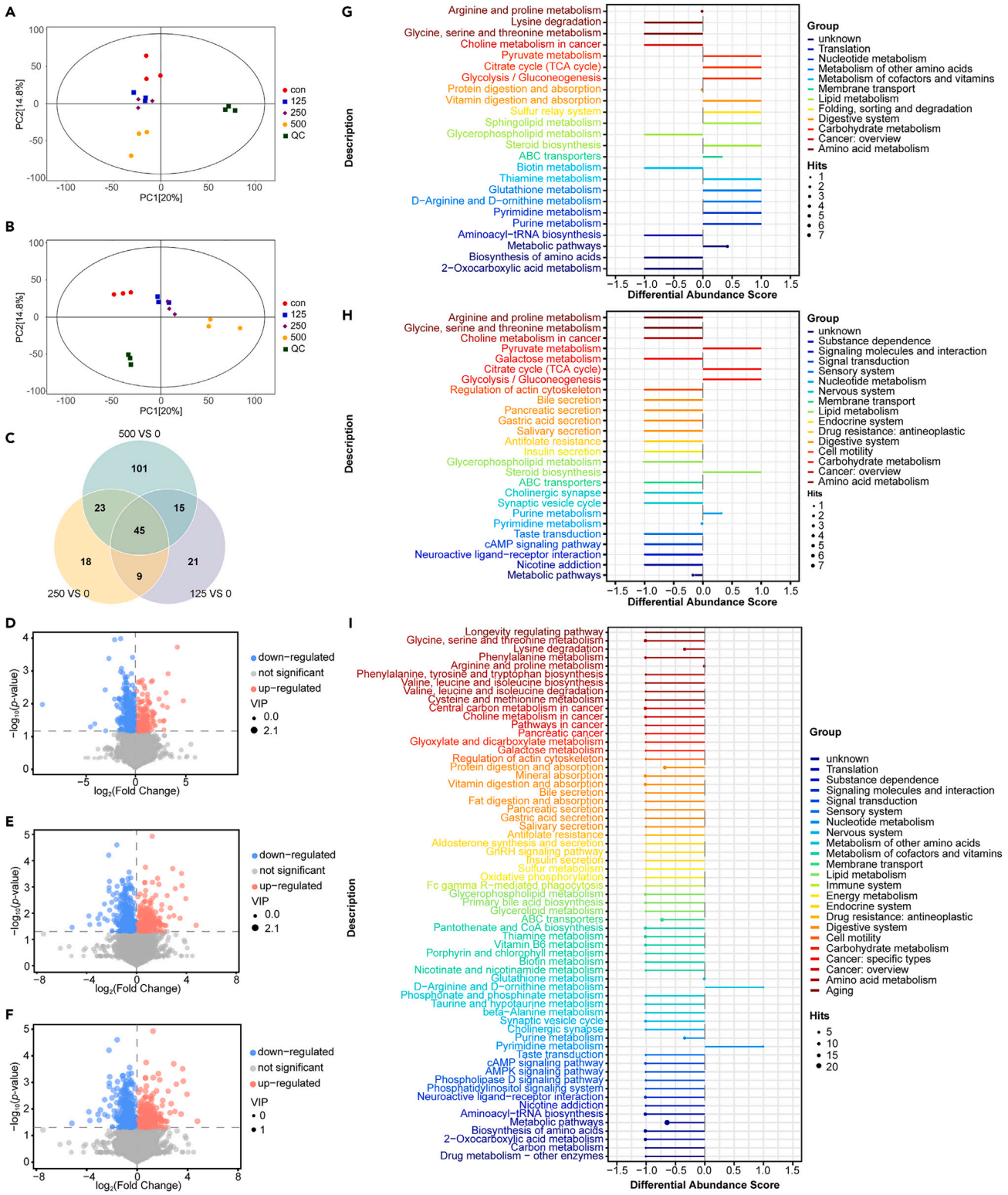
A
PC2[14.8%]
PC1[20%]
con
125
250
500
QC
B
PC2[14.8%]
PC1[20%]
con
125
250
500
QC
C
500 VS 0
101
23
15
45
18
21
9
250 VS 0
125 VS 0
D
−log10(p-value)
log2(Fold Change)
down−regulated
not significant
up−regulated
VIP
0.0
2.1
E
−log10(p-value)
log2(Fold Change)
down−regulated
not significant
up−regulated
VIP
0.0
2.1
F
−log10(p-value)
log2(Fold Change)
down−regulated
not significant
up−regulated
VIP
0
1
G
Description
Arginine and proline metabolism
Lysine degradation
Glycine, serine and threonine metabolism
Choline metabolism in cancer
Pyruvate metabolism
Citrate cycle (TCA cycle)
Glycolysis / Gluconeogenesis
Protein digestion and absorption
Vitamin digestion and absorption
Sulfur relay system
Sphingolipid metabolism
Glycerophospholipid metabolism
Steroid biosynthesis
ABC transporters
Biotin metabolism
Thiamine metabolism
Glutathione metabolism
D−Arginine and D−ornithine metabolism
Pyrimidine metabolism
Purine metabolism
Aminoacyl−tRNA biosynthesis
Metabolic pathways
Biosynthesis of amino acids
2−Oxocarboxylic acid metabolism
Differential Abundance Score
Group
unknown
Translation
Nucleotide metabolism
Metabolism of other amino acids
Metabolism of cofactors and vitamins
Membrane transport
Lipid metabolism
Folding, sorting and degradation
Digestive system
Carbohydrate metabolism
Cancer: overview
Amino acid metabolism
Hits
1
2
3
4
5
6
7
H
Description
Arginine and proline metabolism
Glycine, serine and threonine metabolism
Choline metabolism in cancer
Pyruvate metabolism
Galactose metabolism
Citrate cycle (TCA cycle)
Glycolysis / Gluconeogenesis
Regulation of actin cytoskeleton
Bile secretion
Pancreatic secretion
Gastric acid secretion
Salivary secretion
Antifolate resistance
Insulin secretion
Glycerophospholipid metabolism
Steroid biosynthesis
ABC transporters
Cholinergic synapse
Synaptic vesicle cycle
Purine metabolism
Pyrimidine metabolism
Taste transduction
cAMP signaling pathway
Neuroactive ligand−receptor interaction
Nicotine addiction
Metabolic pathways
Differential Abundance Score
Group
unknown
Substance dependence
Signaling molecules and interaction
Signal transduction
Sensory system
Nucleotide metabolism
Nervous system
Membrane transport
Lipid metabolism
Endocrine system
Drug resistance: antineoplastic
Digestive system
Cell motility
Carbohydrate metabolism
Cancer: overview
Amino acid metabolism
Hits
1
2
3
4
5
6
7
I
Description
Longevity regulating pathway
Glycine, serine and threonine metabolism
Lysine degradation
Phenylalanine metabolism
Arginine and proline metabolism
Phenylalanine, tyrosine and tryptophan biosynthesis
Valine, leucine and isoleucine biosynthesis
Valine, leucine and isoleucine degradation
Cysteine and methionine metabolism
Central carbon metabolism in cancer
Choline metabolism in cancer
Pathways in cancer
Pancreatic cancer
Glyoxylate and dicarboxylate metabolism
Galactose metabolism
Regulation of actin cytoskeleton
Protein digestion and absorption
Mineral absorption
Vitamin digestion and absorption
Bile secretion
Fat digestion and absorption
Pancreatic secretion
Gastric acid secretion
Salivary secretion
Antifolate resistance
Aldosterone synthesis and secretion
GnRH signaling pathway
Insulin secretion
Sulfur metabolism
Oxidative phosphorylation
Fc gamma R−mediated phagocytosis
Glycerophospholipid metabolism
Primary bile acid biosynthesis
Glycerolipid metabolism
ABC transporters
Pantothenate and CoA biosynthesis
Thiamine metabolism
Vitamin B6 metabolism
Porphyrin and chlorophyll metabolism
Biotin metabolism
Nicotinate and nicotinamide metabolism
Glutathione metabolism
D−Arginine and D−ornithine metabolism
Phosphonate and phosphinate metabolism
Taurine and hypotaurine metabolism
beta−Alanine metabolism
Synaptic vesicle cycle
Cholinergic synapse
Purine metabolism
Pyrimidine metabolism
Taste transduction
cAMP signaling pathway
AMPK signaling pathway
Phospholipase D signaling pathway
Phosphatidylinositol signaling system
Neuroactive ligand−receptor interaction
Nicotine addiction
Aminoacyl−tRNA biosynthesis
Metabolic pathways
Biosynthesis of amino acids
2−Oxocarboxylic acid metabolism
Carbon metabolism
Drug metabolism − other enzymes
Differential Abundance Score
Group
unknown
Translation
Substance dependence
Signaling molecules and interaction
Signal transduction
Sensory system
Nucleotide metabolism
Nervous system
Metabolism of other amino acids
Metabolism of cofactors and vitamins
Membrane transport
Lipid metabolism
Immune system
Energy metabolism
Endocrine system
Drug resistance: antineoplastic
Digestive system
Cell motility
Carbohydrate metabolism
Cancer: specific types
Cancer: overview
Amino acid metabolism
Aging
Hits
5
10
15
20

Figure 4. Metabolomic identification of differentially expressed metabolites after Mn exposure to SH-SY5Y cells and analysis of KEGG differential abundance analysis

PCA score plots of QC samples in the ESI^+ mode (A) and ESI^- mode (B) ion modes among 0, 125, 250, and 500 μM $MnCl_2$ exposure. Intersection analysis of DEMs in each treatment group (C), and DEMs after 125, 250, and 500 μM $MnCl_2$ exposure compared to the control, respectively (D–F). KEGG differential abundance scores of DEMs 125 μM (G), 250 μM (H), and 500 μM (I) $MnCl_2$ exposure compared to the control.

the LS/MS data, resulting in 7,395 and 5,261 peaks in the ESI^+ and ESI^- modes, respectively. Furthermore, qualitative identification was performed using publicly available databases and several comprehensive databases. A total of 638 metabolites were identified in the ESI^+ mode, and 320 metabolites were identified in the ESI^- mode. We combined the metabolites identified in ESI^+ and ESI^- ion mode and considered metabolites satisfying both VIP $\geq$ 1 and $p<0.05$ as differentially expressed metabolites (DEMs). The Venn diagrams depicted the 45 DEMs consistent across all exposure conditions (Figure 4C), and the volcano plot showed 90, 95, and 184 DEMs for each treatment group compared to the control (Figures 4D–4F).

The KEGG database was used to obtain the pathway information of the metabolites involved. Compared with the control group, the differential metabolites in the 125 μM exposed group was mainly enriched and affected the metabolic pathways of amino acids, sugars, lipids, energy, and nucleotides, mostly promoting the up-regulation of metabolic pathways (Figure 4G). In the 250 μM exposed group, DEMs affected the nervous system, digestive system, endocrine system, and other metabolic pathways, and the pathways such as amino acids, sugars, lipids, energy, and nucleotide metabolism were gradually inhibited (Figure 4H). DEMs in 500 μM $MnCl_2$-exposed cells were mainly enriched in metabolic pathways associated with cancer and neurodegenerative diseases, and normal physiological functions such as biosynthesis and metabolism were comprehensively inhibited (Figure 4I). Some metabolic pathways such as amino acid metabolism, lipid metabolism, carbohydrate metabolism, and energy metabolism were consistent with the above result from single-cell sequencing.

Metabolic pathway enrichment analysis was performed for the differentially expressed metabolites in each exposure group. As shown in Figure 5A, the metabolic pathways that were significantly affected by exposure included glutathione metabolism, purine metabolism, glycine, serine and threonine metabolism, among which the effect on glutathione metabolism was the most significant. And shown in Figures 5 B–5D, the abundance of three related metabolites in this metabolic pathway was significantly changed. The abundance of GSH and Gly decreased gradually with the increase of Mn exposure concentration, while Glu increased slightly in 125 μM Mn exposure group, and Glu decreased gradually with the increase of Mn exposure concentration. Meanwhile, using VIP $\geq$ 1 as the screening criterion of critical metabolites, we found that Mn had an inhibitory effect on metabolites related to the glutathione metabolic pathway compared to the control group. The 125 μM Mn exposure resulted in a VIP of 1.508 for GSH, 1.533 for Gly and 0.293 for Glu; the 250 μM Mn exposure caused a VIP of 1.709 for GSH, 1.380 for Gly and 0.402 for Glu; and the 500 μM Mn exposure group led to a VIP of 1.596 for GSH, 1.447 for Glu, and 1.377 for Gly. These results suggest that glutathione metabolism is a key metabolic pathway disturbed by Mn neurotoxicity.

Therefore, we validated the metabolomic results in Mn-exposed SH-SY5Y cells. As shown in Figure 6A, GSH levels were significantly inhibited after Mn exposure compared to the control group. In contrast, GSSG levels were significantly elevated with Mn exposure. Glu concentration showed a dose-dependent decrease with the treatment dose of Mn, while Gly concentration kept almost unchanged after Mn exposure (Figures 6B and 6C). Collectively, Mn could inhibit the expression of GSH and Glu in the glutathione metabolic pathway.

Gln reversed Mn neurotoxicity by eliciting UPR^{mt}

For Mn could inhibit the expression of GSH and promote the expression of GSSH, we further use Gln as supplementation to observe the change in GSH and GSSG concentration, and the results showed that Gln alleviated the extent of GSH inhibition (Figure 7A) and alleviated the promoting effect of Mn on GSSG (Figure 7B). We also detected the effects of Gln supplementation on cellular activity and mitochondrial function. As shown in Figure 7C, Gln supplementation reversed the effect of Mn exposure on cellular activity, especially after supplementation with 8 mM Gln. Meanwhile, ROS levels and proportion of MMP depolarization (Q3) showed a significant decrease after Gln supplementation (Figures 7D and 7E), compared with the same treatment dose of Mn without the Gln supplementation group. The above results

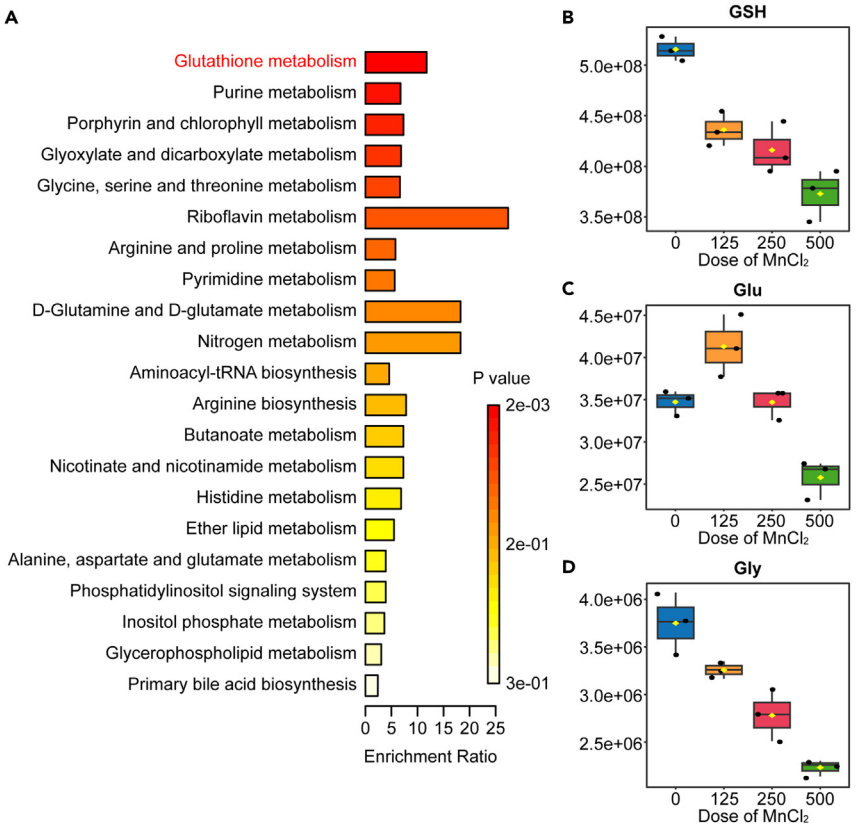

Figure 5. Metabolic pathway enrichment analysis for differentially expressed metabolites after Mn exposure to SH-SY5Y cells

(A) Metabolic pathway analysis of differentially expressed metabolites that were significantly altered in each exposure group. Abundance of metabolites associated with the glutathione metabolic pathway, GSH (B), Glu (C), and Gly (D).

indicated that Gln supplementation could effectively increase GSH levels and reverse the neurotoxic damage of Mn on cell activity and mitochondrial function.

As we mentioned above, UPR^{mt} is an important mechanism in Mn neurotoxicity, we further observed the change of expression levels of UPR^{mt}-related proteins with the existence of Gln supplementation. Figure 8 revealed that Gln supplementation attenuated the inhibition of UPR^{mt}-related protein chop and clpp expression by Mn. Especially, Gln supplementation has a significant effect on the expression of lonp1. The expression of lonp1 showed an increasing trend in the 4 mM Gln group, which was in contrast with the 2 mM Gln group. Although 8 mM Gln supplementation also increased the lonp1 concentration, the extent was lower than in the 4 mM Gln group. These findings implied that Gln supplementation could reverse the inhibitory effect of Mn on UPR^{mt} and attenuate the neurotoxicity of Mn.

DISCUSSION

In the present study, we performed single-cell sequencing of zebrafish brain tissue and identified differentially expressed genes in DA neurons, which were mainly involved in mitochondrial amino acid metabolism and protein misfolding. We further used a non-targeted metabolomics approach to screen the potential metabolites and found that Mn could inhibit the expression of GSH and Glu in the glutathione metabolic pathway. Mechanistically, we found that Gln supplementation could enhance GSH levels and trigger UPR^{mt} which could rescue redox imbalance and mitochondrial dysfunction to counteract the neurotoxicity of Mn. Our current study provided a previously unidentified mechanism by which Gln supplementation could reverse Mn neurotoxicity. Moreover, our results provided evidence that Gln supplementation might be a potential therapy for Mn-related neurological disorders.

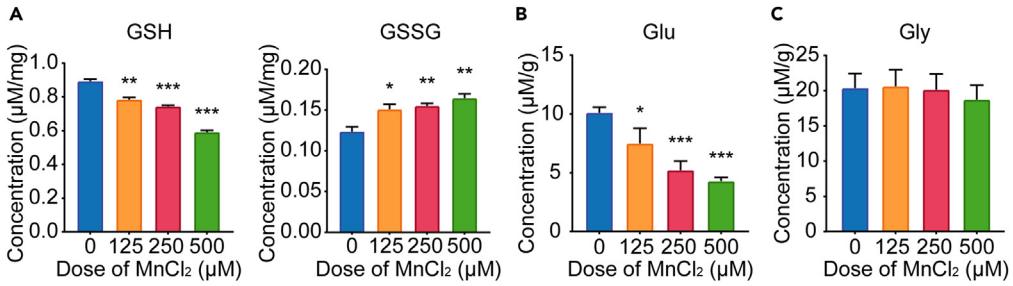

Figure 6. Mn exposure affected glutathione metabolism in SH-SY5Y cells

The expression levels of related metabolites GSH and GSSG(A), Glu(B), and Gly(C) was assessed using GSH and GSSG assay kit, glutamic acid content assay kit, and glycine ELISA kit and measured by a microplate reader. All data are presented as means ± SD, n = 3. *$p < 0.05$, **$p < 0.01$, ***$p < 0.001$ versus the control.

Manganism is a neurological disorder that exhibits certain motor symptoms similar to PD, and meta-analyses indicate that Mn levels are significantly elevated in PD patients.[21] Previous studies suggested that the mechanism of Mn neurotoxicity includes mitochondrial dysfunction, redox homeostasis, and altering neurotransmitter metabolism.[22,23] Our results of single-cell sequencing of zebrafish brain tissue also showed that a large number of differentially expressed genes in DA neurons after Mn exposure were associated with amino acids, energy metabolism, unfolded protein, and electron respiratory transport chains.

To dig out the specific metabolites changed by Mn exposure, we used a non-targeted metabolomics approach to screen the potential metabolites and found that Mn could inhibit the expression of GSH and Glu in the Gln metabolic pathway, which was consistent with previous studies. A cross-sectional study observed significant negative correlations of blood Glu with blood Mn and the behavioral cognitive deficit index in preschool children.[24] Glu is a component of GSH, an oxidative scavenger that is widely present in neuronal mitochondria.[12] Mn can interfere with the synthesis of GSH and lead to increased GSSG levels and oxidative damage.[13] In previous studies, GSH deficiency enhances Mn-induced mitochondrial dysfunction because of oxidative stress and DA depletion-induced neurotoxicity in rat striatal.[25] Evidence suggests that depletion of GSH exacerbated neuronal death, whereas increased intracellular GSH activity prevented MPP^+-induced apoptosis in SH-SY5Y cells.[26] Similarly, the knockdown of GSH reduced mitochondrial performance, ATP levels are reduced, and mitochondrial oxygen consumption is decreased.[27]

GSH is synthesized from Glu, Gly, and cysteine (Cys). Studies have shown that under stimulated conditions, mitochondrial ROS levels are elevated and GSH is deficient, leading to intracellular accumulation of misfolded proteins and ultimately to apoptosis.[28] Therefore, we speculate that mitochondrial dysfunction such as redox imbalance because of GSH depletion may affect UPR^{mt}. Studies have shown that GSH supplements are not the most effective option, but supplementation with their constituent amino acids may enhance GSH synthesis.[29,30] Supplementing Gly and N-acetylcysteine (GlyNAC) in aged mice improves naturally occurring GSH deficiency and mitochondrial impairment. GlyNAC supplementation for 24 weeks in older adults corrected mitochondrial dysfunction, and improved cognition, gait speed, and exercise capacity.[31] Clinical data provide evidence that Gln supplementation reduces mortality, and infection rates in critically ill patients and patients undergoing major surgery.[32] Gln is the most abundant nonessential amino acid in the human body and the only one that can directly pass the cerebrovascular barrier.[11] Gln, which can be converted into Glu and ammonia by glutaminase in cells, is often used as a supplement for Glu, and at the same time is an important nitrogen source in cells. Nitrogen is a precursor to the synthesis of amino acids, proteins, and nucleic acids. Studies have shown that Gln is most effective in increasing GSH levels during GSH depletion.[33] Similar to these data, we effectively increased the expression level of GSH in SH-SY5Y cells after Mn exposure by Gln supplementation, which was accompanied by enhanced cell viability and improved mitochondrial function. It has also been shown that excessive Mn exposure can disrupt glutamine and glutamate transporter interactions in glial cells.[34] However, in the present study, we found that GSH concentration was significantly increased after Gln supplementation, indicating that exogenous Gln supplementation can indeed affect cellular GSH metabolism. In addition, our results also showed that when supplemented with a certain dose of Gln, the concentration of GSH in the Mn-exposed group was still significantly lower than that in the non-exposed group. This result indirectly

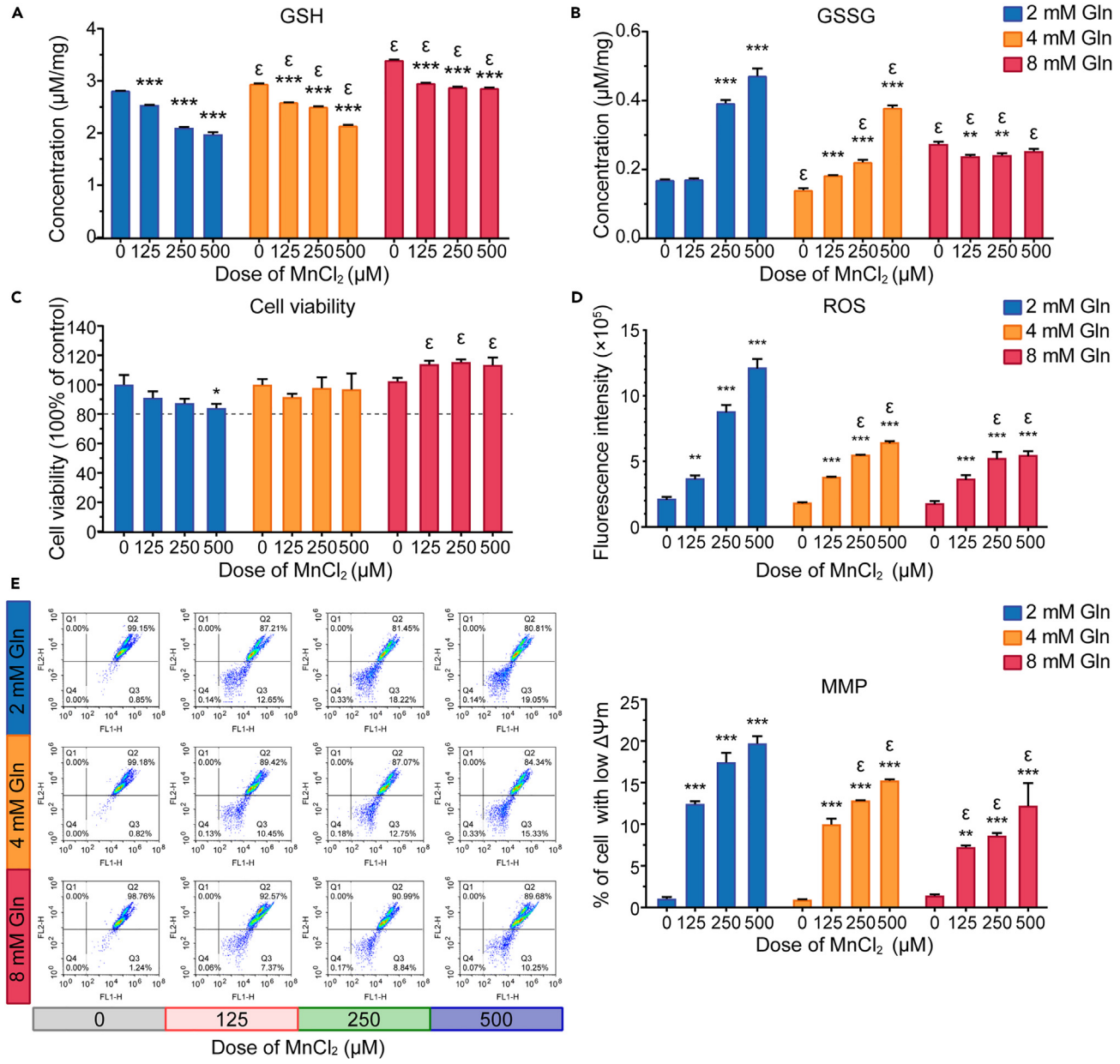

Figure 7. Gln supplementation increased GSH levels and reversed Mn neurotoxicity by eliciting UPR^{mt}

The effects of Gln supplementation on GSH (A), GSSG (B), cellular viability (C), ROS levels (D), and MMP (E) in Mn-exposed SH-SY5Y cells. The concentrations of GSH and GSSG was assessed using GSH and GSSG assay kit and measured by a microplate reader (n = 3). The cell viability was assessed using CCK kit and measured by a microplate reader (n = 6). The levels of ROS and MMP were measured using flow cytometry (n = 3). All data are presented as means ± SD. *$p < 0.05$, **$p < 0.01$, ***$p < 0.001$ versus the untreated group, $^{\varepsilon}p<0.05$, versus the 2 mM Gln group.

indicated that Mn exposure had a damaging effect on key enzymes or proteins in the pathway of conversion of Gln to Glu or synthesis of GSH by Glu.

Consistent postmortem neuropathological studies suggest that oxidative stress and abnormal protein aggregation are the main features of Mn neurotoxicity, but the underlying mechanisms have not been fully elucidated.[35] However, in the present study, we found that Mn exposure could inhibit UPR^{mt}, which may be a main reason for abnormal protein aggregation induced by Mn neurotoxicity. To maintain mitochondrial physiological function, the mitochondria develop the UPR^{mt} as a specific repair pathway.[36] UPR^{mt}

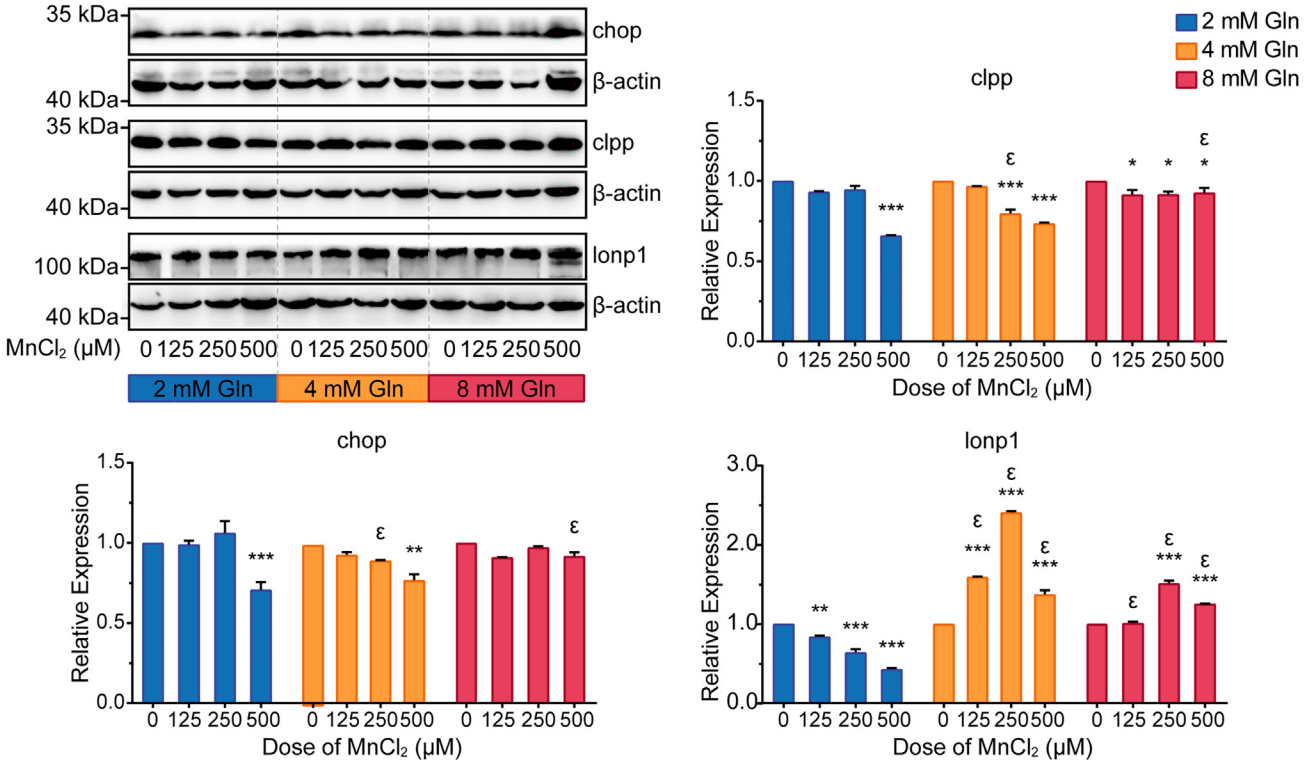

Figure 8. Gln supplementation reversed the inhibitory effect of Mn on UPR^{mt}

The relative expression levels of UPR^{mt}-related proteins (chop, clpp, and lonp1) were used for western blot and were quantified using ImageJ. All data are presented as mean ± SD, n = 3. *$p < 0.05$, **$p < 0.01$, ***$p < 0.001$ versus the untreated group, $^{\varepsilon}p<0.05$, versus the 2 mM Gln group.

prevents abnormal protein accumulation within the mitochondria via the normalization of mitochondrial protein folding and degradation.[37] UPR^{mt} activation is critical to ensure normal development, for it plays an important role in inducing metabolic adaptation and mitochondrial recovery.[38]

To explore the potential mechanism of the neuroprotective effect of GSH increase, we focused on the response to unfolded protein enriched by DEGs in DA neurons after Mn exposure. We observed that after supplementation with Gln, Mn had a reduced inhibitory effect on the UPR^{mt} pathway and an activating effect on lonp1-mediated UPR^{mt}, and reduced mitochondrial dysfunction. However, no direct interaction between GSH and UPR^{mt} has been reported before. Nevertheless, it has been shown that the antioxidant enzyme GSH-Px and the heat shock proteins HSP90, HSP70, and HSP60 synergistically prevent apoptosis in heat stress-induced hepatocyte injury.[39] Serum levels of GSH and Hsp60 were positively correlated during neonatal stress.[40] As studies have reported that these heat shock proteins are key molecular chaperone proteins of UPR^{mt}.[41,42] Also, there are studies on the correlation between NAD^+ and UPR^{mt}, which has a redox capacity similar to that of GSH. In a model of cardiac hypertrophy, niacinamide nucleoside promotes the expression of chop, clpp, and lonp1, resulting in further activation of UPR^{mt}, which effectively alleviates reduced mitochondrial oxygen consumption and cardiomyocyte death.[43] Therefore, we postulated that boosting GSH levels in neurons could activate UPR^{mt} and repair mitochondrial biological function. Meanwhile, we are not able to exclude that UPR^{mt} may affect the synthesis of GSH which still need to be studied.

In our study, the expressions of mitochondrial chaperone protein clpp and mitochondrial protease lonp1 were significantly suppressed after Mn exposure to SH-SY5Y cells, whereas the expression of chop was activated after low-dose Mn exposure and subsequently inhibited. Nevertheless, multiple studies confirmed up-regulation of the UPR^{mt}-related mRNA in mitochondrial disease,[44] which may be directly related to the different processes of the integrated mitochondrial stress response (ISR^{mt}). The early ISR^{mt} is autonomous cellular protection homeostasis against metabolic damage, with lonp1-activated expression and

slight inhibition of clpp, which is not identical to our study. The second stage activates serine and glutathione synthesis and affects tissue and systemic metabolic changes, corroborating our previous metabolomics results. The terminal stage shows significant activation of the transcription factor CHOP and mild induction of mitochondrial heat shock protein. Remarkably, ISR^{mt} is an initial protective mechanism of the organism and there was no major neuronal damage, which may explain the inconsistency of our obtained results with previous studies.

Taken together, our results suggest a previously unrealized mechanism that Gln supplementation can increase GSH levels to trigger UPR^{mt} which can rescue redox imbalance and mitochondrial dysfunction induced by Mn and counteract Mn neurotoxicity. Our study highlights Gln supplementation as a therapeutic approach in Mn-related neurological disorders.

Limitations of the study

In summary, increasing GSH levels in neurons can trigger UPR^{mt} and reverse mitochondrial dysfunction. However, we cannot exclude that UPR^{mt} may affect the synthesis of GSH, and the regulatory relationship between UPR^{mt} and GSH awaits further exploration.

STAR★METHODS

Detailed methods are provided in the online version of this paper and include the following:

- KEY RESOURCES TABLE
- RESOURCE AVAILABILITY
  - Lead contact
  - Materials availability
  - Data and code availability
- EXPERIMENTAL MODEL AND STUDY
  - Experimental models
  - Zebrafish maintenance and exposure
  - Neurobehavioral tests of zebrafish
  - Histological analysis and single-cell sequencing
  - Cells culture
  - Cell viability assay
  - Metabolomic assay sample collection
  - Western blot analysis
  - Determination of glutamate, glycine, and glutathione concentrations
  - Detection of ROS and MMP
- QUANTIFICATION AND STATISTICAL ANALYSIS

SUPPLEMENTAL INFORMATION

Supplemental information can be found online at https://doi.org/10.1016/j.isci.2023.107136.

ACKNOWLEDGMENTS

This study was supported by the National Natural Science Foundation of China, China (81973007, 82103797), the R&D Program of Beijing Municipal Education Commission, China (KM202210025026), and Young Elite Scientist Sponsorship Program by BAST, China (BYESS2023385).

AUTHOR CONTRIBUTIONS

Conceptualization, S.Z., J.L., and P.N.; methodology, S.Z.; validation, S.Z.; formal analysis, S.Z. and J.Z.; investigation, S.Z. and J.Z.; data curation, S.Z. and L.W.; writing–original draft, S.Z. and J.L.; writing–review and editing, J.L. and L.C.; supervision, P.N. and J.L.; funding acquisition, P.N. and J.L.

DECLARATION OF INTERESTS

The authors declare no conflict of interest.

INCLUSION AND DIVERSITY

We support inclusive, diverse, and equitable conduct of research.

Received: February 15, 2023
Revised: May 24, 2023
Accepted: June 12, 2023
Published: June 15, 2023

REFERENCES

1. Kenborg, L., Lassen, C.F., Hansen, J., and Olsen, J.H. (2012). Parkinson's disease and other neurodegenerative disorders among welders: a Danish cohort study. Mov. Disord. *27*, 1283–1289. https://doi.org/10.1002/mds.25125.

2. Budinger, D., Barral, S., Soo, A.K.S., and Kurian, M.A. (2021). The role of manganese dysregulation in neurological disease: emerging evidence. Lancet Neurol. *20*, 956–968. https://doi.org/10.1016/S1474-4422(21)00238-6.

3. Jenkitkasemwong, S., Akinyode, A., Paulus, E., Weiskirchen, R., Hojyo, S., Fukada, T., Giraldo, G., Schrier, J., Garcia, A., Janus, C., et al. (2018). SLC39A14 deficiency alters manganese homeostasis and excretion resulting in brain manganese accumulation and motor deficits in mice. Proc. Natl. Acad. Sci. USA *115*, E1769–E1778. https://doi.org/10.1073/pnas.1720739115.

4. Lee, E.Y., Flynn, M.R., Du, G., Lewis, M.M., Kong, L., Yanosky, J.D., Mailman, R.B., and Huang, X. (2019). Higher hippocampal mean diffusivity values in asymptomatic welders. Toxicol. Sci. *168*, 486–496. https://doi.org/10.1093/toxsci/kfz011.

5. Horning, K.J., Caito, S.W., Tipps, K.G., Bowman, A.B., and Aschner, M. (2015). Manganese Is Essential for Neuronal Health. Annu. Rev. Nutr. *35*, 71–108. https://doi.org/10.1146/annurev-nutr-071714-034419.

6. Benedetto, A., Au, C., and Aschner, M. (2009). Manganese-induced dopaminergic neurodegeneration: insights into mechanisms and genetics shared with Parkinson's disease. Chem. Rev. (Washington, DC, U. S.) *109*, 4862–4884. https://doi.org/10.1021/cr800536y.

7. Lin, M., Colon-Perez, L.M., Sambo, D.O., Miller, D.R., Lebowitz, J.J., Jimenez-Rondan, F., Cousins, R.J., Horenstein, N., Aydemir, T.B., Febo, M., and Khoshbouei, H. (2020). Mechanism of manganese dysregulation of dopamine neuronal activity. J. Neurosci. *40*, 5871–5891. https://doi.org/10.1523/JNEUROSCI.2830-19.2020.

8. Zhang, Z., Yan, J., Bowman, A.B., Bryan, M.R., Singh, R., and Aschner, M. (2020). Dysregulation of TFEB contributes to manganese-induced autophagic failure and mitochondrial dysfunction in astrocytes. Autophagy *16*, 1506–1523. https://doi.org/10.1080/15548627.2019.1688488.

9. Lu, J., Li, Y., Zhang, C., Yang, X., and Qiang, J. (2022). Metabolic changes of the reduction of manganese intake in the hepatic encephalopathy rat: NMR- and MS-based metabolomics study. Biometals *35*, 935–953. https://doi.org/10.1007/s10534-022-00415-3.

10. Fernandes, J., Chandler, J.D., Liu, K.H., Uppal, K., Hao, L., Hu, X., Go, Y.M., and Jones, D.P. (2019). Metabolomic responses to manganese dose in SH-SY5Y human neuroblastoma cells. Toxicol. Sci. *169*, 84–94. https://doi.org/10.1093/toxsci/kfz028.

11. Cruzat, V., Macedo Rogero, M., Noel Keane, K., Curi, R., and Newsholme, P. (2018). Glutamine: Metabolism and immune function, supplementation and clinical translation. Nutrients *10*, 1564. https://doi.org/10.3390/nu10111564.

12. Ricke, K.M., Paß, T., Kimoloi, S., Fährmann, K., Jüngst, C., Schauss, A., Baris, O.R., Aradjanski, M., Trifunovic, A., Eriksson Faelker, T.M., et al. (2020). Mitochondrial dysfunction combined with high calcium load leads to impaired antioxidant defense underlying the selective loss of nigral dopaminergic neurons. J. Neurosci. *40*, 1975–1986. https://doi.org/10.1523/JNEUROSCI.1345-19.2019.

13. da Silva Santos, V., Bisen-Hersh, E., Yu, Y., Cabral, I.S.R., Nardini, V., Culbreth, M., Teixeira da Rocha, J.B., Barbosa, F., Jr., and Aschner, M. (2014). Anthocyanin-rich acai (Euterpe oleracea Mart.) extract attenuates manganese-induced oxidative stress in rat primary astrocyte cultures. J. Toxicol. Environ. Health *77*, 390–404. https://doi.org/10.1080/15287394.2014.880392.

14. Martins, A.C., Gubert, P., Li, J., Ke, T., Nicolai, M.M., Moura, A.V., Bornhorst, J., Bowman, A.B., and Aschner, M. (2022). *Caenorhabditis elegans* as a model to study manganese-induced neurotoxicity. Biomolecules *12*, 1396. https://doi.org/10.3390/biom12101396.

15. Mohandas, G., Rao, S.V., Muralidhara, and Rajini, P.S. (2017). Whey protein isolate enrichment attenuates manganese-induced oxidative stress and neurotoxicity in Drosophila melanogaster: Relevance to Parkinson's disease. Biomed. Pharmacother. *95*, 1596–1606. https://doi.org/10.1016/j.biopha.2017.09.099.

16. Kwon, O.K., Kim, S.J., Lee, Y.M., Lee, Y.H., Bae, Y.S., Kim, J.Y., Peng, X., Cheng, Z., Zhao, Y., and Lee, S. (2016). Global analysis of phosphoproteome dynamics in embryonic development of zebrafish (*Danio rerio*). Proteomics *16*, 136–149. https://doi.org/10.1002/pmic.201500017.

17. Rubin, S.A., Baron, C.S., Pessoa Rodrigues, C., Duran, M., Corbin, A.F., Yang, S.P., Trapnell, C., and Zon, L.I. (2022). Single-cell analyses reveal early thymic progenitors and pre-B cells in zebrafish. J. Exp. Med. *219*, e20220038. https://doi.org/10.1084/jem.20220038.

18. Nabinger, D.D., Altenhofen, S., Bitencourt, P.E.R., Nery, L.R., Leite, C.E., Vianna, M.R.M.R., and Bonan, C.D. (2018). Nickel exposure alters behavioral parameters in larval and adult zebrafish. Sci. Total Environ. *624*, 1623–1633. https://doi.org/10.1016/j.scitotenv.2017.10.057.

19. Kachot, R.L., Patel, U.D., Patel, H.B., Modi, C.M., Chauhan, R., Kariya, M.H., and Bhadaniya, A.R. (2023). Neurotoxicity of acrylamide in adult zebrafish following short-term and long-term exposure: evaluation of behavior alterations, oxidative stress markers, expression of antioxidant genes, and histological examination of the brain and eyes. Environ. Sci. Pollut. Res. Int. *30*, 40116–40131. https://doi.org/10.1007/s11356-022-25112-z.

20. Fiore, N.J., Tamer-Mahoney, J.D., Beheshti, A., Nieland, T.J.F., and Kaplan, D.L. (2022). 3D biocomposite culture enhances differentiation of dopamine-like neurons from SH-SY5Y cells: A model for studying Parkinson's disease phenotypes. Biomaterials *290*, 121858. https://doi.org/10.1016/j.biomaterials.2022.121858.

21. Du, K., Liu, M.Y., Pan, Y.Z., Zhong, X., and Wei, M.J. (2018). Association of circulating manganese levels with Parkinson's disease: a meta-analysis. Neurosci. Lett. *665*, 92–98. https://doi.org/10.1016/j.neulet.2017.11.054.

22. Soares, A.T.G., Silva, A.d.C., Tinkov, A.A., Khan, H., Santamaría, A., Skalnaya, M.G., Skalny, A.V., Tsatsakis, A., Bowman, A.B., Aschner, M., and Ávila, D.S. (2020). The impact of manganese on neurotransmitter systems. J. Trace Elem. Med. Biol. *61*, 126554. https://doi.org/10.1016/j.jtemb.2020.126554.

23. Martinez-Finley, E.J., Gavin, C.E., Aschner, M., and Gunter, T.E. (2013). Manganese neurotoxicity and the role of reactive oxygen species. Free Radic. Biol. Med. *62*, 65–75. https://doi.org/10.1016/j.freeradbiomed.2013.01.032.

24. He, B., Wang, Y., Li, S., Zhao, Y., Ma, X., Wang, W., Li, X., and Zhang, Y. (2021). A cross-sectional survey of preschool children: Exploring heavy metal exposure, neurotransmitters, and neurobehavioural relationships and mediation effects.

Ecotoxicol. Environ. Saf. *220*, 112391. https://doi.org/10.1016/j.ecoenv.2021.112391.

25. Desole, M.S., Esposito, G., Migheli, R., Sircana, S., Delogu, M.R., Fresu, L., Miele, M., de Natale, G., and Miele, E. (1997). Glutathione deficiency potentiates manganese toxicity in rat striatum and brainstem and in PC12 cells. Pharmacol. Res. *36*, 285–292. https://doi.org/10.1006/phrs.1997.0197.

26. Wang, G., Ma, W., and Du, J. (2018). β-Caryophyllene (BCP) ameliorates MPP+ induced cytotoxicity. Biomed. Pharmacother. *103*, 1086–1091. https://doi.org/10.1016/j.biopha.2018.03.168.

27. Jha, N., Jurma, O., Lalli, G., Liu, Y., Pettus, E.H., Greenamyre, J.T., Liu, R.M., Forman, H.J., and Andersen, J.K. (2000). Glutathione depletion in PC12 results in selective inhibition of mitochondrial complex I activity. Implications for Parkinson's disease. J. Biol. Chem. *275*, 26096–26101. https://doi.org/10.1074/jbc.M000120200.

28. El Dor, M., Dakik, H., Polomski, M., Haudebourg, E., Brachet, M., Gouilleux, F., Prié, G., Zibara, K., and Mazurier, F. (2020). VAS3947 induces UPR-mediated apoptosis through cysteine thiol alkylation in AML cell lines. Int. J. Mol. Sci. *21*, 5470. https://doi.org/10.3390/ijms21155470.

29. Valencia, E., Marin, A., and Hardy, G. (2002). Impact of oral L-glutamine on glutathione, glutamine, and glutamate blood levels in volunteers. Nutrition *18*, 367–370. https://doi.org/10.1016/s0899-9007(02)00774-8.

30. Gould, R.L., and Pazdro, R. (2019). Impact of supplementary amino acids, micronutrients, and overall diet on glutathione homeostasis. Nutrients *11*, 1056. https://doi.org/10.3390/nu11051056.

31. Kumar, P., Liu, C., Hsu, J.W., Chacko, S., Minard, C., Jahoor, F., and Sekhar, R.V. (2021). Glycine and N-acetylcysteine (GlyNAC) supplementation in older adults improves glutathione deficiency, oxidative stress, mitochondrial dysfunction, inflammation, insulin resistance, endothelial dysfunction, genotoxicity, muscle strength, and cognition: Results of a pilot clinical trial. Clin. Transl. Med. *11*, e372. https://doi.org/10.1002/ctm2.372.

32. Bollhalder, L., Pfeil, A.M., Tomonaga, Y., and Schwenkglenks, M. (2013). A systematic literature review and meta-analysis of randomized clinical trials of parenteral glutamine supplementation. Clin. Nutr. *32*, 213–223. https://doi.org/10.1016/j.clnu.2012.11.003.

33. Matés, J.M., Campos-Sandoval, J.A., de Los Santos-Jiménez, J., and Márquez, J. (2020). Glutaminases regulate glutathione and oxidative stress in cancer. Arch. Toxicol. *94*, 2603–2623. https://doi.org/10.1007/s00204-020-02838-8.

34. Sidoryk-Wegrzynowicz, M., Lee, E., Mingwei, N., and Aschner, M. (2011). Disruption of astrocytic glutamine turnover by manganese is mediated by the protein kinase C pathway. Glia *59*, 1732–1743. https://doi.org/10.1002/glia.21219.

35. Harischandra, D.S., Ghaisas, S., Zenitsky, G., Jin, H., Kanthasamy, A., Anantharam, V., and Kanthasamy, A.G. (2019). Manganese-induced neurotoxicity: new insights into the triad of protein misfolding, mitochondrial impairment, and neuroinflammation. Front. Neurosci. *13*, 654. https://doi.org/10.3389/fnins.2019.00654.

36. Zhu, L., Luo, X., Fu, N., and Chen, L. (2021). Mitochondrial unfolded protein response: a novel pathway in metabolism and immunity. Pharmacol. Res. *168*, 105603. https://doi.org/10.1016/j.phrs.2021.105603.

37. Shpilka, T., Du, Y., Yang, Q., Melber, A., Uma Naresh, N., Lavelle, J., Kim, S., Liu, P., Weidberg, H., Li, R., et al. (2021). UPR(mt) scales mitochondrial network expansion with protein synthesis via mitochondrial import in Caenorhabditis elegans. Nat. Commun. *12*, 479. https://doi.org/10.1038/s41467-020-20784-y.

38. Nargund, A.M., Fiorese, C.J., Pellegrino, M.W., Deng, P., and Haynes, C.M. (2015). Mitochondrial and nuclear accumulation of the transcription factor ATFS-1 promotes OXPHOS recovery during the UPR(mt). Mol. Cell. *58*, 123–133. https://doi.org/10.1016/j.molcel.2015.02.008.

39. Sun, J., Liu, Z., Quan, J., Li, L., Zhao, G., and Lu, J. (2021). Protective effects of different concentrations of selenium nanoparticles on rainbow trout (Oncorhynchus mykiss) primary hepatocytes under heat stress. Ecotoxicol. Environ. Saf. *230*, 113121. https://doi.org/10.1016/j.ecoenv.2021.113121.

40. Giuffrè, M., Rizzo, M., Scaturro, G., Pitruzzella, A., Marino Gammazza, A., Cappello, F., Corsello, G., and Li Volti, G. (2015). Oxidative stress markers at birth: Analyses of a neonatal population. Acta Histochem. *117*, 486–491. https://doi.org/10.1016/j.acthis.2015.01.007.

41. Kumar, R., Chaudhary, A.K., Woytash, J., Inigo, J.R., Gokhale, A.A., Bshara, W., Attwood, K., Wang, J., Spernyak, J.A., Rath, E., et al. (2022). A mitochondrial unfolded protein response inhibitor suppresses prostate cancer growth in mice via HSP60. J. Clin. Invest. *132*, e149906. https://doi.org/10.1172/JCI149906.

42. Münch, C., and Harper, J.W. (2016). Mitochondrial unfolded protein response controls matrix pre-RNA processing and translation. Nature (Lond.) *534*, 710–713. https://doi.org/10.1038/nature18302.

43. Smyrnias, I., Gray, S.P., Okonko, D.O., Sawyer, G., Zoccarato, A., Catibog, N., López, B., González, A., Ravassa, S., Díez, J., and Shah, A.M. (2019). Cardioprotective effect of the mitochondrial unfolded protein pesponse during chronic pressure overload. J. Am. Coll. Cardiol. *73*, 1795–1806. https://doi.org/10.1016/j.jacc.2018.12.087.

44. Forsström, S., Jackson, C.B., Carroll, C.J., Kuronen, M., Pirinen, E., Pradhan, S., Marmyleva, A., Auranen, M., Kleine, I.M., Khan, N.A., et al. (2019). Fibroblast growth factor 21 drives dynamics of local and systemic stress responses in mitochondrial myopathy with mtDNA deletions. Cell Metabol. *30*, 1040–1054.e7. https://doi.org/10.1016/j.cmet.2019.08.019.

45. Darland, T., and Dowling, J.E. (2001). Behavioral screening for cocaine sensitivity in mutagenized zebrafish. Proc. Natl. Acad. Sci. USA *98*, 11691–11696. https://doi.org/10.1073/pnas.191380698.

46. Zhong, S., Ding, W., Sun, L., Lu, Y., Dong, H., Fan, X., Liu, Z., Chen, R., Zhang, S., Ma, Q., et al. (2020). Decoding the development of the human hippocampus. Nature (Lond.) *577*, 531–536. https://doi.org/10.1038/s41586-019-1917-5.

47. Cosacak, M.I., Bhattarai, P., Reinhardt, S., Petzold, A., Dahl, A., Zhang, Y., and Kizil, C. (2019). Single-cell transcriptomics analyses of neural stem cell heterogeneity and contextual plasticity in a zebrafish brain model of amyloid toxicity. Cell Rep. *27*, 1307–1318.e3. https://doi.org/10.1016/j.celrep.2019.03.090.

48. Sun, X.L., Chen, B.Y., Zhao, H.K., Cheng, Y.Y., Zheng, M.H., Duan, L., Jiang, W., and Chen, L.W. (2016). Gas1 up-regulation is inducible and contributes to cell apoptosis in reactive astrocytes in the substantia nigra of LPS and MPTP models. J. Neuroinflammation *13*, 180. https://doi.org/10.1186/s12974-016-0643-2.

STAR★METHODS

KEY RESOURCES TABLE

REAGENT or RESOURCE	SOURCE	IDENTIFIER
Antibodies		
Anti-Rabbit β-Actin	Cell Signaling Technology	RRID:AB_2223172
Anti-Rabbit CHOP	Proteintech	RRID:AB_2292610
Anti-Rabbit CLPP	Abcam	RRID:AB_10975619
Anti-Rabbit LONP1	Abcam	RRID:AB_10975619
Anti-Rabbit IgG	Jackson ImmunoResearch	RRID:AB_2313567
Chemicals, peptides, and recombinant proteins		
DMEM, high glucose	Gibco	11960-044
Fetal Bovine Serum	Gibco	10270-106
L-Glutamine (200mM)	Gibco	25030-081
Sodium pyruvate (100mM)	Gibco	11360-070
Trypsin-EDTA (0.25%)	Gibco	25200-056
Phosphate Buffered Saline (1×)	KeyGEN BioTECH	KGB5001
RIPA	Beyotime	P0013B
Critical commercial assays		
Cell Counting Kit	Zomanbio	ZP328
Enhanced BCA Protein Assay Kit	Beyotime	P0010
Reactive Oxygen Species Assay Kit	KeyGEN BioTECH	KGT010-1
JC-10 Apoptosis Detection Kit	KeyGEN BioTECH	KGA605-KGA608
GSH and GSSG Assay Kit	Beyotime	S0053
Glutamic Acid Content Assay Kit	Solarbio	BC1585
Glycine ELISA Kit	ELK Biotechnology	ELK8276
Experimental models: Cell lines		
SH-SY5Y	Cell Resource Center of Peking Union Medical College	N/A
Software and algorithms		
Loupe Browser 5.0	Loupe Browser Software	https://www.10xgenomics.com/products/loupe-browser/
R 4.1.1	R software	https://www.r-project.org/
Cytoscape 3.9.0	Cytoscape Software	https://cytoscape.org/
GraphPad Prism 9	GraphPad Software	https://www.graphpad.com/scientific-software/prism/

RESOURCE AVAILABILITY

Lead contact

Further information and requests for resources and reagents should be directed to and will be fulfilled by the lead contact: Jie Li (lijie46@ccmu.edu.cn).

Materials availability

This study did not generate new unique reagents.

Data and code availability

- All data will be shared upon request to the lead contact. No standardized datatype data were generated in this study.

- This study did not generate new code.
- Any additional analysis information for this work is available by request to the lead contact.

EXPERIMENTAL MODEL AND STUDY

Experimental models

AB strain adult (6 months old) wild-type female and male zebrafish (*Danio rerio*) and human neuroblastoma SH-SY5Y cells.

Zebrafish maintenance and exposure

Wild-type zebrafish (*Danio rerio*) of the AB strain were purchased from the China Zebrafish Resource Center. The adult zebrafish (6 months old, half males and females) were first acclimated to the experimental conditions for a week. Then zebrafish were randomly transferred to aquaria (only males or females per aquarium) and reared using filtered and dechlorinated water maintained at a pH between 7.0 and 7.4, with continuous aeration. In the experiment, male and female zebrafish were exposed to 0, 0.25, 1, and 4 mg/L of $MnCl_2$ for 30 d, respectively. During the period of acclimation and experimentation, zebrafish were maintained under a 14 h light and 10 h dark photoperiod cycle at 28.5 ± 1°C, fed twice daily with brine shrimp, and the water was renewed every 24 h. The experimental protocol was approved by the Ethics Committee of Capital Medical University (ethical review number: AEEI-2022-161).

Neurobehavioral tests of zebrafish

After exposure, zebrafish from each treated group (10 males and 10 females) were transferred separately to clear water without $MnCl_2$ for a T-maze experiment. The T-maze assay was conducted according to the protocol defined by Darland, T[45] with some modifications. The T-maze apparatus used in this study includes one long arm and two short arms, one of which opened into a large reservoir, deeper than the rest of the maze, and placed 10 heterosexual zebrafish, defining this area as the enrichment chamber (EC) zone. The experimental test included three stages. The first was acclimation, the entire group of zebrafish was placed in the T-maze and allowed to swim freely for 2 h for 4 d. Subsequently training, each zebrafish was placed in the start zone and released after 30 s, allowed to swim freely for 4 min for 4 d, and the fish would be rewarded with food if they found the EC zone. Finally testing, the protocol was the same as the training, evaluated and analyzed zebrafish swimming trajectory by using the Danio Vision behavioral equipment (Genostar, Beijing, China).

Histological analysis and single-cell sequencing

After 30 d of Mn exposure, the zebrafish were anesthetized with ice water for 1 min to record the body weight after removing residual moisture. Afterward, zebrafish brain tissue samples were fixed in the 4% paraformaldehyde fix solution, next dehydrated, embedded in paraffin, and sectioned under a rotatory microtome (5 μm). Finally, the samples were stained with the hematoxylin and eosin (HE) technique for further analysis. Brain tissues from three additional zebrafish in each group were dissected into single-cell suspensions and sent to OE Biotech Co., Ltd (Shanghai, China) for single-cell sequencing. Seurat package was used to read sequencing data and perform t-SNE clustering analysis. First, we removed all ribosomal RNA genes, and then we filtered out the following cells: cells with less than 800 or more than 7000 unique genes and cells with more than 15% mitochondrial genes.[46] The data were normalized using the 'LogNormalize' method, and the data were scaled by scalefactor = 10^4. The cell clusters with higher resolution = 1.0 were displayed using t-SNE.[47] By using some general markers, we identified 10 major cell types. Finally, we used differentially expressed genes (DEGs) of DA neurons for GO analysis and KEGG pathway analysis with a p-value<0.05 as the threshold.

Cells culture

The SH-SY5Y cells were purchased from the Cell Resource Center of Peking Union Medical College. The cells were cultured in the complete medium consisting of high-glucose Dulbecco's Modified Eagle Medium (DMEM) supplemented with 10% fetal bovine serum, 1 mM sodium pyruvate, and 2 mM Gln, kept at 37°C with 5% CO_2 for 36-48 h.[48] Cells with a logarithmic growth phase and 80% growth density were selected for passaging culture. First discarded the original complete medium, and washed the cells twice with phosphate-buffered saline (PBS), then treated with 0.25% trypsin for 1 min, immediately terminated the digestion with serum-containing medium and collected the cells by centrifugation at 1000 rpm for 5 min, and finally seeded into new complete culture medium at a ratio of 1:3 to keep culturing.

Cell viability assay

SH-SY5Y cells were inoculated into 96-well plates with a quantity of 1×10^4/well with 100 μL complete medium for 24 h. After that, the cells were treated with different doses of $MnCl_2$ (0, 62.5, 125, 250, 500, and 1000 μM) for 3, 6, 12, and 24 h with six replicate wells. To measure cell viability, we used the CCK kit for the assay according to standard protocol. The absorbance was determined at 450 nm using a microplate reader.

Metabolomic assay sample collection

After exposure to 0, 125, 250, and 500 μM $MnCl_2$ for 6 h, SH-SY5Y cells were digested with 0.25% trypsin for 1 min, then cells were collected by centrifugation at 1000 rpm for 5 min. We then washed cells twice with PBS to remove the serum and finally resuspended cells with 1 mL PBS. For rapid counting, 1×10^7 cells from each group were taken as samples and immediately stored in liquid nitrogen and handed over to Biotree biomedical technology Co., Ltd. (Shanghai, China) for the determination of non-targeted metabolomics. All the groups were derived from triplicate experiments.

Western blot analysis

SH-SY5Y cells were collected with a cell scraper after exposure to Mn. Total proteins were extracted by RIPA buffer supplemented with protease inhibitors. After protein quantification using the BCA protein assay kit, equal amounts of total proteins were subjected to SDS-PAGE and transferred onto nitrocellulose membranes (Bio-Rad Laboratories), which were blocked in 5% non-fat milk, and incubated with primary antibodies against chop (1:200, Proteintech, 15204-1-AP), clpp (1:1000, Abcam, ab124822), lonp1 (1:200, Abcam, ab103809), and β-actin (1:1000, Cell Signaling Technology, 4970) overnight. Subsequently, the membranes were treated with HRP-conjugated secondary antibodies (1:5000, Cell Signaling Technology, 7074) for 1 h. The protein signals were visualized using enhanced chemiluminescence and further analyzed by Image J software (NIH, Bethesda, MD, USA).

Determination of glutamate, glycine, and glutathione concentrations

The concentrations of Glu, glycine (Gly), GSH and oxidized glutathione (GSSG) were detected using Glutamic Acid Content Assay Kit (Solarbio), Glycine ELISA Kit (ELK Biotechnology), and the GSH and GSSG Assay Kit (Beyotime) according to the manufacturer's protocol, respectively. The absorbances for Glu, Gly, and total glutathione (GSSG and GSH) were detected at 340 nm, 450 nm, and 412 nm, respectively. The concentration of GSSG could be determined by removing GSH from the sample with appropriate reagents. The concentration of GSH could be calculated by subtracting GSSG from the total glutathione.

Detection of ROS and MMP

The logarithmically growing cells were inoculated into 6-well plates with a quantity of 3×10^5/well and treated with 0, 125, 250, and 500 μM $MnCl_2$ for 6 h. Subsequently, ROS levels were detected using the Reactive Oxygen Species Assay Kit (KeyGEN BioTECH). DCFH-DA was diluted with serum-free DMEM at 1:1000 to reach a final concentration of 10 μmol/L. After removing the medium, cells were washed 3 times with PBS, and 1 mL diluted DCFH-DA probe was added. Following incubation for 20 min at 37°C, the cells were washed with PBS to fully remove DCFH-DA. The fluorescence intensity of 10,000 cells was detected by flow cytometry under the FITC channel. Simultaneously, changes in mitochondrial membrane potential were detected with the JC-10 Apoptosis Detection Kit (KeyGEN BioTECH). The treated cells were collected by trypsinization and then labeled with JC-10 for 30 min at 37°C. Polarized mitochondria in the aggregate form and depolarized mitochondria in the monomeric form were stained with green and orange fluorescence, respectively. Thus, green and orange emission light were analyzed by fluorescence channel 1 (FL1) and fluorescence channel 2 (FL2) using flow cytometry, respectively.

QUANTIFICATION AND STATISTICAL ANALYSIS

Significant differences were evaluated by student's t-test, one-way analysis of variance (ANOVA), and Tukey posthoc test depending on the experimental design. All results were derived from triplicate experiments and presented as mean ± SD. Statistically significant differences are indicated as $*p<0.05$, $**p<0.01$, $***p<0.001$. All graphics were made using GraphPad PRISM (version 9.0). Single-cell transcriptome sequencing and metabolome results were analyzed and visualized with R software (version 4.1.1), Loupe Browser (version 5.0), and Cytoscape (version 3.7.2).